Effect of A-site cation ordering on oxygen diffusion in NdBa2Fe3O8 through molecular dynamics

Milad Moazzam, Chenyi Li, Giulio Cordaro, Guilhem Dezanneau

Effect of A-site cation ordering on oxygen diffusion in $NdBa_2Fe_3O_8$ through Molecular Dynamics

Milad Moazzam, Chenyi Li, Giulio Cordaro, Guilhem Dezanneau*

Laboratoire Structures, Propriétés et Modélisation des Solides, UMR8580 CNRS / CentraleSupélec, Université Paris-Saclay, 8 Rue Joliot Curie, 91190 Gif-sur-Yvette, France

Abstract :

$RE_{1+x}Ba_{2-x}Fe_3O_{8+\delta}$ (*RE* = Pr, Nd, Sm, …) have been presented recently as potential electrode materials for Solid Oxide Fuel Cells. Depending on the composition, these materials may present a disordered cubic perovskite phase, an ordered quintuple perovskite or a mixing of both. Such an evolution in the structure potentially affects oxygen ion diffusion at the core of the air electrode property. In the present study based on molecular dynamics simulations, we explore the influence of cation order on oxygen diffusion properties. We determine both macroscopic diffusion coefficients and also extract some information about atomic scale mechanisms. Similarly to previous results on double cobaltites, we explore if the disordering of A-site cations favours or not oxygen diffusion in these ferrites. We finally show that the nano-ordering, as observed experimentally, leads to a slight improvement of the oxygen ions diffusion process compared to the fully ordered structure, having its oxygen diffusion coefficient much smaller than the one of the disordered structure.

*corresponding author:

G. Dezanneau, guilhem.dezanneau@centralesupelec.fr

Introduction

The search for more efficient Solid Oxide Fuel Cells has led researchers to explore a wide range of original compositions, particularly for electrodes, mainly based on perovskite-type oxides. Manganites were historically explored first and present a very high electron conductivity and good catalytic properties. However, their low oxide-ion conductivity supposes to develop electrodes with original microstructure to obtain a high density of triple-phase boundaries and high performance [1-3]. Cobaltites usually also present a high electron conductivity and a significant oxygen diffusion coefficient resulting in remarkable electrochemical properties. However, they appear less robust than other compositions due to a higher reactivity and a thermal expansion mismatch with electrolyte materials leading to mechanical degradation [4-7]. In addition, the presence of cobalt introduces health, social and environmental concerns [8-9]. Ferrites also present a mixed ion-electron conductivity, but electronic conductivity is usually smaller (compared to cobaltites and manganites), and their catalytic properties are worse than those of cobaltites [10-13]. Ferrites are nevertheless more stable and, in some cases, can even withstand hydrogen-containing atmospheres making them potentially interesting for symmetrical SOFCs [14-16]. On the other hand, several works report that layered compounds may also present high-performance properties, where the layered structure is expected to favour an anisotropic oxygen diffusion [17]. Among these layered compounds, double cobaltites have been widely studied due to their exceptional electrochemical properties [18-23]. Attempts to prepare double perovskite manganites or ferrites led to much more difficulties. For instance, the synthesis of the double perovskite oxide $YBaMn_2O_{5+\delta}$ was shown to require low oxygen partial pressure conditions to prevent the formation of $BaMnO_{3-\delta}$ [24-26]. Single crystals with composition $REBaMn_2O_{5+\delta}$ (*RE* = Y, Sm, Eu, Gd, Tb, Dy) could also be prepared using low oxygen partial pressure conditions [27]. Double perovskite ferrites have also been studied, but several studies indicate difficulty stabilising the double perovskite structure in air conditions [28-30]. Following this idea to obtain perovskite-based compounds with A-site ordering, researchers explored several new compositions, for instance, the materials based on YBaCuO-type compounds [31-33] and more recently, the $RE_{2-x}Ba_{3+x}Fe_5O_{15-\delta}$ (*RE* = Y, Pr, Nd, Sm, Eu, Gd) series of compounds with promising air-electrode properties [34-37]. In this last case, a quintuple perovskite phase was revealed, even for compositions close to $NdBa_2Fe_3O_{8+\delta}$, for which a triple perovskite structure could have been expected [38-39]. A specific sandwich structure was proposed in which A-sites cations alternate following the sequence Nd / Ba / (Nd, Ba) / (Nd, Ba) / Ba, i.e., a layered structure in which pure Nd or Ba layers alternate with disordered layers.

Based on our previous experience with double perovskite cobaltite modelling, molecular dynamics (MD) can be an efficient tool to correlate macroscopic diffusion properties to the local specific

ordering of atoms. In particular, we demonstrated that, in the double perovskite compound $NdBaCo_2O_{5+\delta}$, the oxygen diffusion occurs mainly through jumps from the Nd to the Co planes (and reciprocally), while Ba planes act as barriers. Our objective in the present study was to identify whether the specific ordering observed in quintuple perovskite could enhance diffusion properties and how the nano-ordering, as revealed experimentally, may also affect oxygen diffusion coefficients. Our study relies on molecular dynamics calculations. We evaluate the macroscopic diffusion coefficients for different types of ordered/disordered $NdBa_2Fe_3O_8$ compounds and make the correlation between such diffusion coefficients and local diffusion mechanisms.

II. Calculations details

II.1. Molecular dynamics simulation

As mentioned above, Molecular Dynamics (MD) calculations were previously applied with success to other cathode materials like *RE*$BaCo_2O_{5.5}$ (*RE* = Y, La, Nd, Gd) [18-19]. We used the same type of simulations here. In particular, MD simulations were performed using the DLPOLY Classic code [40] using a supercell of 10×10×10 perovskite unit cells containing 333 Nd, 666 Ba, 1000 Fe and 2667 O atoms, corresponding thus to the nominal composition $NdBa_2Fe_3O_8$. The oxygen stoichiometry was fixed at 8 atoms per formula unit, even if experiments report values between 7.8 and 8.3 at 900 °C, depending on oxygen partial pressure [35]. This fixed oxygen composition allows selecting a formal charge of +3 for iron atoms. The composition used for simulations thus contains a constant oxygen content, although such compound is shown to lose oxygen in the air as temperature increases [39]. Therefore our system with constant stoichiometry will allow us to obtain reliable information about the diffusion mechanisms but may present intrinsic errors in reproducing the experimental evolution of diffusion coefficient with temperature, as could be obtained from tracer or relaxation measurements.

During our simulations, the interactions between ions were described by a long-range Coulombic term calculated by Ewald summation and a short-range Buckingham pair potential. For Coulombic interactions, the formal charges +3, +2, +3 and −2 were used respectively for Nd, Ba, Fe and O ions. The use of standard ionic charge was shown to describe the dynamical features of atoms correctly in most oxide compounds. The Buckingham potential is defined by:

$$\varphi_{ij}(r) = A_{ij} \exp\left(-\frac{r}{\rho_{ij}}\right) - \frac{C_{ij}}{r^6} \qquad (3)$$

Where *r* is the distance between the atoms *i* and *j*, and A_{ij}, ρ_{ij} and C_{ij} are potential parameters specific to each ion pair whose values are given in Table 2. The set of potentials was taken from previous studies [18; 41], which were shown to reproduce oxide materials' properties.

Interaction	A (eV)	ρ (Å)	C (eV.Å^6)
Nd^{3+} - O^{2-}	1379.90	0.36072	22.59
Ba^{2+} - O^{2-}	1214.40	0.3522	0.0
Fe^{3+} - O^{2-}	1156.36	0.3299	0.0
O^{2-} - O^{2-}	22764.3	0.149	43.00

Table 2. Inter-atomic Buckingham potentials used for molecular dynamics calculations. M-O interactions are taken from: Ba-O [18], Fe-O [41], Nd-O [18], O-O [18; 41].

During these simulations, the system was first equilibrated at temperatures between 1500 and 2000 K and at zero pressure for 40,000 timesteps with a time step of 1 fs in the isothermal-isobaric (NσT) ensemble with the Nosé-Hoover thermostat. Afterwards, the equilibrium lattice parameters were calculated with 100,000 timesteps more. Then, simulations were performed in the NVT mode during 50,000 timesteps after 10,000 equilibration steps. Finally, NVE simulations were realised during 3,500,000 timesteps, corresponding to a simulation time of 3.5 ns. General information deduced from the obtained trajectories was analysed using the code NMOLDYN 3.08 [42] and home-made analysis codes.

II.2. Configurations

The different configurations studied in this work are represented in Figure 1:

- **Disordered configurations (**Figure 1.a**):** the disordered configurations correspond to the case where Nd and Ba cations are distributed randomly in the structure leading thus logically to a cubic perovskite structure. We studied five configurations of this type corresponding to different Nd/Ba cations distributions and a mean composition $NdBa_2Fe_3O_8$.
- **Quintuple perovskite configuration (**Figure 1.b**):** This configuration is the one proposed for $Nd_{2-x}Ba_{3+x}Fe_3O_{15-\delta}$, where x varies between 0 and 0.5, leading to Nd/Ba ratios between 0.42 and 0.66. For the composition $NdBa_2Fe_3O_8$ considered here, the ratio is 0.5. This configuration is based on an A-site ordering of the perovskite phase along the *c* direction, following the scheme of Nd_1 / Ba_1 / (Nd_2, Ba_2) / (Nd_2, Ba_2) / Ba_1 on A-sites for successive

planes. A 33% Nd and 66% Ba occupancy in mixed Nd_2-Ba_2 planes is used to ensure the correct composition. This specific structure was proposed based on TEM measurements, precisely on the observation in the reciprocal space of the spots at distances equal to the multiples of c*/5 , on the direct imaging of a *5a* periodicity in HAADF-STEM images, and finally on the identification of atomic plane content using STEM-EDX [39].

- **Nano-ordered configurations (**Figure 1.c**):** For these configurations, we assume that the quintuple perovskite structure does not extend more than a few unit cells, beyond which the ordered structure changes of orientation, keeping the Fe and O sublattice coherent. We were interested in evaluating if the nano-ordering observed in TEM experiments and leading to the observation by XRD of a long-range cubic structure (and not a quintuple perovskite) could lead to enhanced diffusion properties. Concretely, each quintuple perovskite subdomain represents here a 5*5*5 block. The total supercell thus contains thus 8 of these blocks with different random orientations. We studied five different configurations of this type.

All these configurations were prepared by combining a homemade code and the Atomsk software [43].

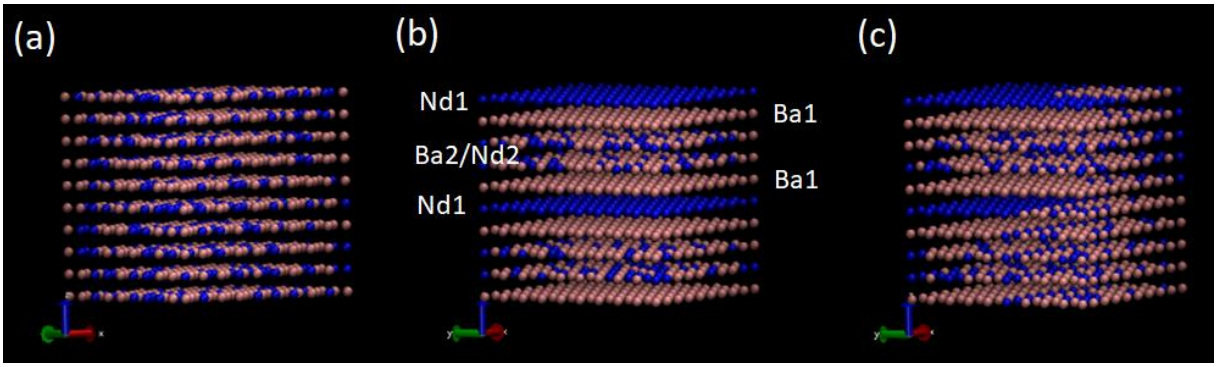

Figure 1. Different configurations studied (a) disordered configuration, (b) quintuple perovskite configuration and (c) nano-ordered configuration. Only Nd and Ba are represented in blue and pink, respectively. Ba_1 and Nd_1 belong to single-element planes, Ba_2 and Nd_2 are located in planes presenting a mixture of both cations.

III. Results and discussion

III.1. Macroscopic results

All the studied configurations were shown to be stable, *i.e.*, even high-temperature simulations did not lead to structure decomposition. We thus deduce that the proposed configurations do not

generate a level of internal stress susceptible to destroying the whole ensemble. As expected, the supercells of disordered configurations remain cubic, while the quintuple perovskite supercell presents a slight tetragonal distortion due to the size of the supercell being longer in the *c* direction compared to the *a* and *b* directions. For example, the size of the quintuple perovskite supercell at 1500 K is 39.45 Å in the *a* and *b* directions, and 39.68 Å in the *c* direction. For nano-ordered configurations, the system naturally evolves toward a triclinic supercell, even if it remains very close to cubic, because the angles of the supercell box never decrease below 89°.

From the simulations, we can follow all the atoms – namely Nd, Ba, Fe, O – and verify if they remain on their site or diffuse throughout the structure. We thus calculated the mean square displacement of all the atoms. As an example, we show in Figure 2 the result of such calculation for the quintuple perovskite configuration. As expected, cations only vibrate around their initial position. On the opposite, oxygen ions tend to move far away from their original position, as shown in Figure 2.b, proving that such material is indeed an oxide ion conductor. We also observe that this square displacement tends to increase with the temperature, in agreement with the fact that diffusion is a thermally activated process.

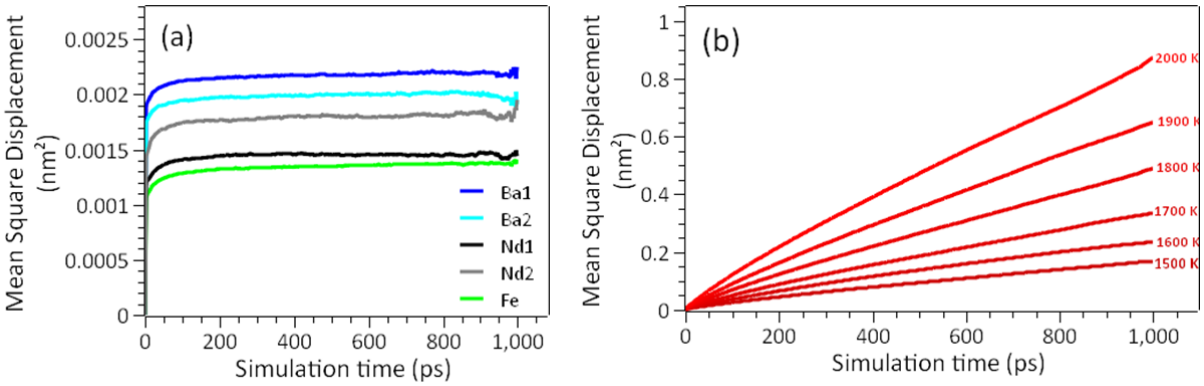

Figure 2. Means square displacements of ions in the quintuple perovskite configurations (a) for cations at 1500 K (b) for oxygen ions at different temperatures.

From these last curves, one can extract the diffusion coefficients as deduced from Einstein's law :

$$MSD(O) = 6 \times D_O \times t \qquad [1]$$

Where MSD(O) is the Mean Square Displacement of oxygen ions, D_O is the oxygen ion diffusion coefficient, t is the simulation time. The oxygen ions diffusion coefficients were extracted for all the configurations and temperatures, and the associated activation energies were calculated (Figure 3).

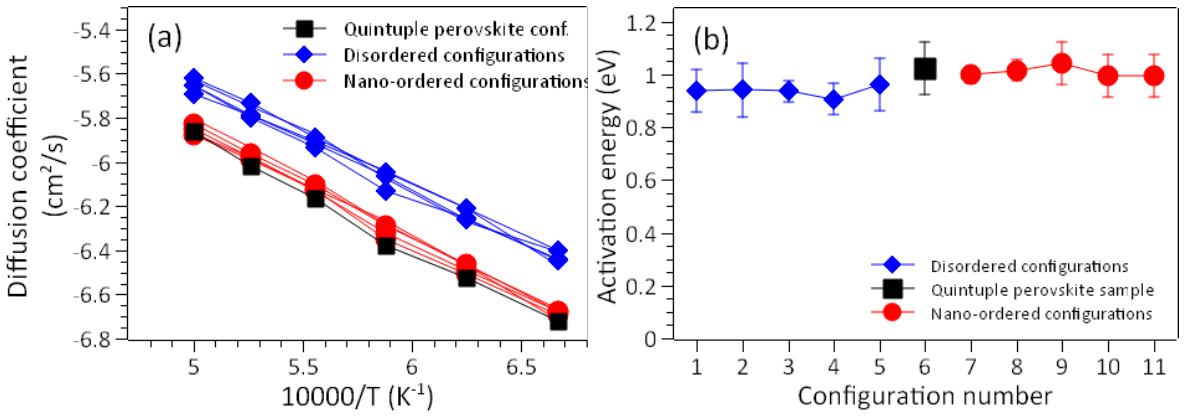

Figure 3. (a) Diffusion coefficients as extracted from MD simulations and (b) associated activation energies

The oxygen ions diffusion coefficients for disordered configurations are always greater than the ones for the quintuple perovskite and nano-ordered phases. This result is somewhat different from to the one observed in double perovskite by Parfitt *et al.* They indeed reported that the total diffusivity of oxygen ions tends to diminish as some disordering is introduced in double perovskite cells [44]. It is worth mentioning that their study did not explore the fully disordered case. In our case, the trend clearly indicates that ordered phases present smaller diffusion coefficients compared to disordered ones. Nevertheless, we notice that the nano-ordering tends to slightly improve the ion diffusion coefficient. The activation energies for each configuration range between 0.9 and 1.1 eV, and are slightly smaller for disordered configurations compared to ordered ones.

Figure 4 shows the evolution of the diffusion coefficients along with the X, Y, Z directions of the supercells at 1500 K, for the different configurations. As expected, disordered configurations do not present much anisotropy, with D_X, D_Y, and D_Z being very similar. On the opposite, in the quintuple perovskite structure, there is more significant diffusion anisotropy: the oxygen diffusion coefficient along with the Z-direction is about 9 times smaller than that along with X and Y directions. Note that the X, Y and Z directions in the quintuple perovskite configurations correspond respectively to the *a*, *b*, and *c* crystallographic axes. Nano-ordered configurations present an intermediate behaviour with eventually some marked anisotropy (not necessarily aligned with Z direction due to the random

orientation of subdomains). In all cases, the anisotropy seen here is not comparable to the extreme one observed in double perovskite, in which the diffusion of oxygen ions across Ba-planes was almost totally impeded [18; 44; 45].

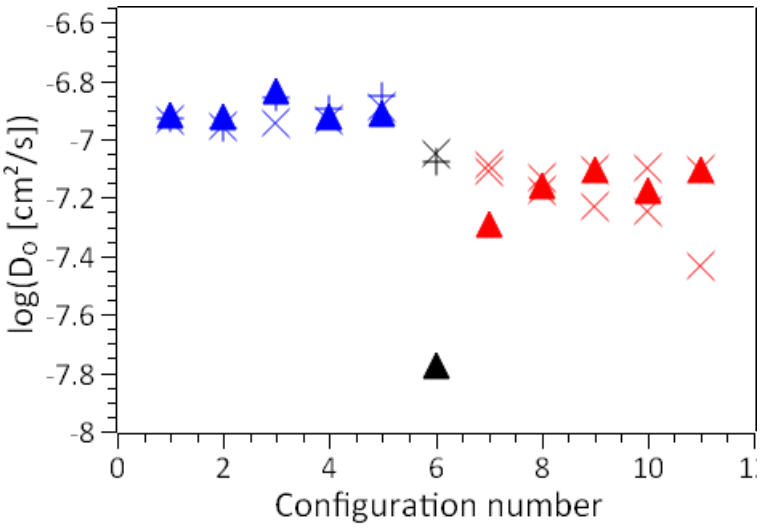

Figure 4. Diffusion coefficients at 1500 K along with *X* direction (✚), *Y* direction (✕), and *Z* direction (▲) for the different configurations (blue: disordered configurations; black: quintuple perovskite configurations; red: nano-ordered configurations) in logarithmic scale.

III.2. Atomic-scale mechanisms

In order to reveal why we observe such an anisotropy in the different materials, in particular the quintuple perovskite configuration, we determined the oxygen 3D density, which was shown to reveal oxygen pathways in previous studies [18]. The oxygen density maps are obtained by refolding all the oxygen positions inside a unit cell or a 1*1*5 supercell, as chosen here for comparison with the ordered configuration. The oxygen density map for the disordered perovskite configuration, shown in Figure 5, is obtained thanks to the software Vesta [46]. It reveals that the presence probability is non-zero between oxygen crystallographic sites, a typical situation when oxygen diffusion occurs. It also shows that no specific orientation appears, as expected for a structure in which Nb and Ba cations are distributed randomly on the A-site. Indeed, the oxygen density map looks very similar, whatever direction is considered (see Figures 5.a, 5.b, and 5.c).

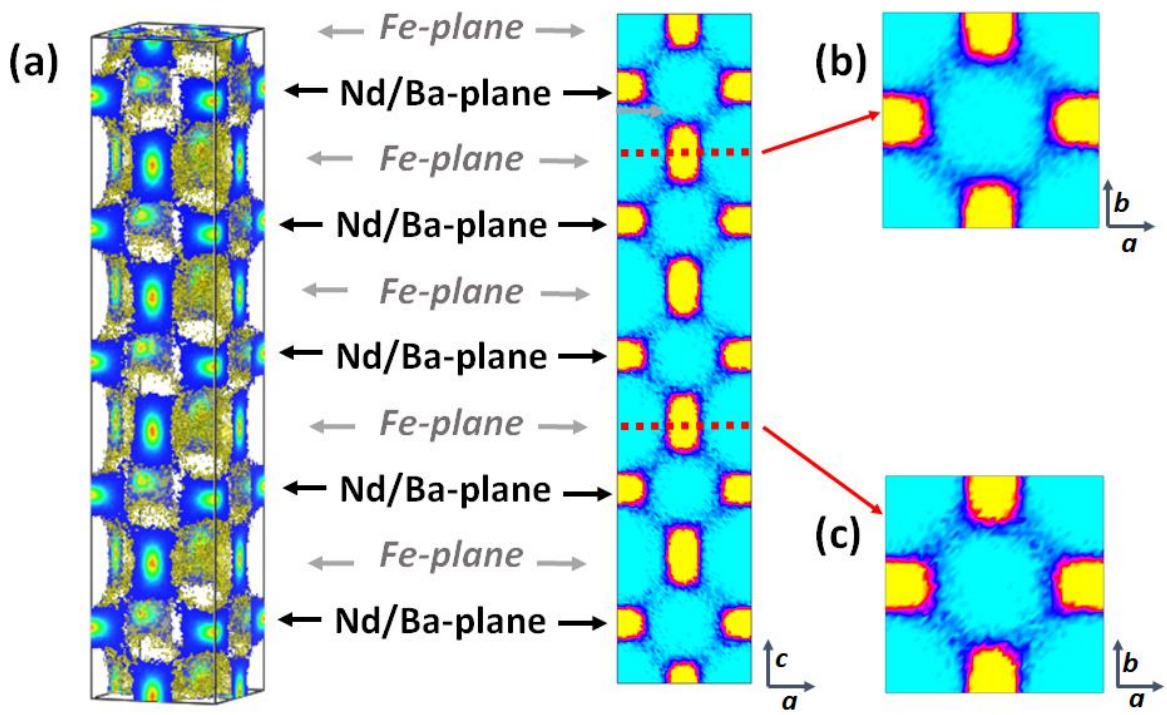

Figure 5. (a) Representation of oxygen ion density 3D and 2D maps showing diffusion pathways in the disordered configuration. Nd/Ba- and Fe-containing planes are identified. (b) and (c) projection of the oxygen density in two Fe-planes.

The oxygen density map for the quintuple perovskite configuration is shown in Figure 6. It reveals that the alternate A-planes forming the quintuple perovskite configuration induce a specific behaviour regarding oxygen diffusivity. In particular, it appears that planes containing only Ba ions act as a barrier for oxygen diffusion, making the long-range diffusion of oxygen ions essentially bi-dimensional, i.e., occurring mainly along the *a* and *b* directions. This result explains the anisotropy of the oxygen diffusion coefficient i.e. the ratio between diffusion coefficient along X and Y directions and the one along the Z direction, for the quintuple perovskite configuration observed at the macroscopic scale (black symbols in Figure 4). Indeed, the diffusion of oxygen ions mainly occurs parallelly through the planes containing Nd cations or a mixture of Nd and Ba cations, as revealed by the non-null presence of oxygen atoms between crystallographic sites (Figure 6.a). Nevertheless, Nd_1-containing planes or Nd_2/Ba_2-containing planes constitute different environments for the oxygen ions. In the first case, Nd_1-containing planes are surrounded by Ba_1-containing planes on both sides. The local structure thus looks like the one observed in double perovskites like $GdBaCo_2O_{5.5}$ [44]. In this case, the movement of oxygen ions follows a zig-zag curve between Nd1- and Fe-containing planes. We can assume that the Co- and Fe-planes act with the same mechanism because the local

structure is very similar. As shown in Figure 6.b., the diffusion of oxygen ions within a Fe-containing plane is very shallow. The mechanism of diffusion is thus involving oxygen ions jumping from an Nd-plane to a Fe-plane and reciprocally, similarly to the one previously reported [16-17]. On the opposite, close to Nd_2/Ba_2-containing planes, the oxygen ions jumps can occur from Nd_2/Ba_2-containing planes to Fe-containing planes, but also within Fe-containing planes, as shown in Figure 6.c. Such a behaviour is thus similar to the one observed for the disordered structure. The main difference between these configurations is that the planes of the disordered structure are interconnected and entirely available for the diffusion of oxygen ions. In contrast, the Ba_1-containing planes of the ordered configuration are not involved in the diffusion process, so they can be seen as unused volume of the lattice and, at the same time, act as a barrier along the Z direction. Such planar anisotropy can be beneficial only if the diffusion through the remaining directions is highly enhanced, but this is not the case for the structure considered in this study. This can explain the higher macroscopic diffusion coefficients obtained for the disordered configuration than the ordered ones (Figure 3.a).

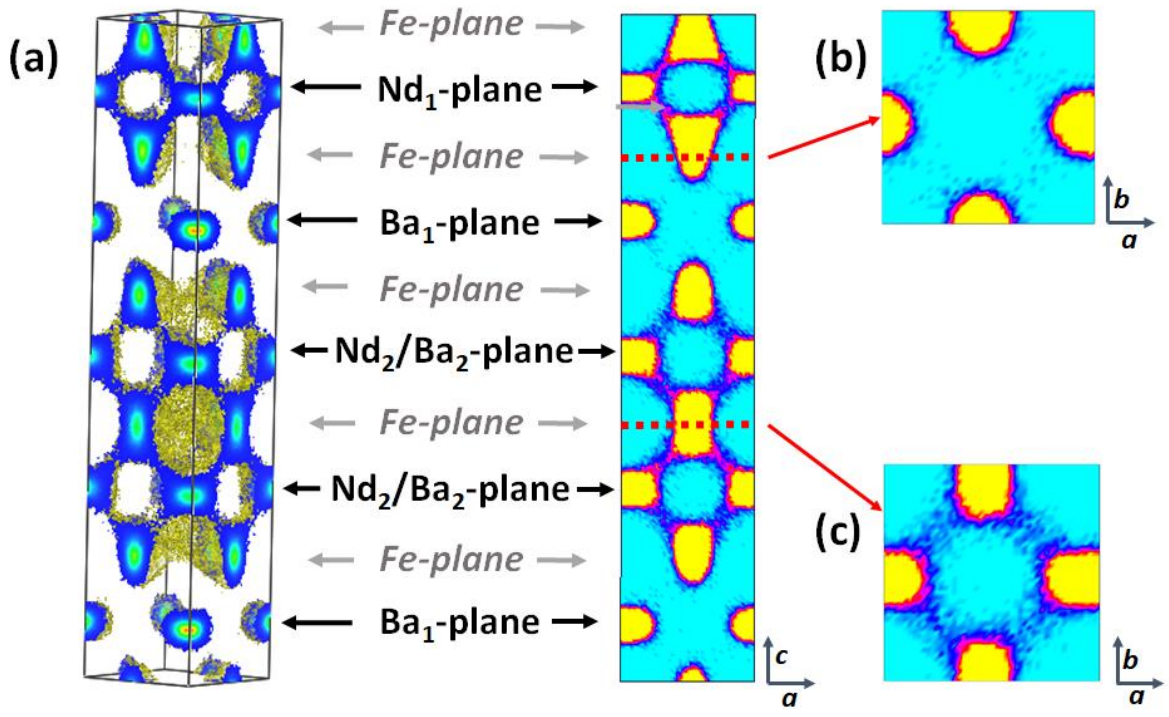

Figure 6. (a) Representation of oxygen ion density 3D and 2D maps showing diffusion pathways in the ordered configuration. Nd- and Ba- containing planes are identified. (b) projection of the oxygen density in a Fe-plane adjacent to an Nd_1-plane (c) projection of the oxygen density in a Fe-plane adjacent to an Nd_2/Ba_2-plane.

IV. Conclusion

In the present work, we have explored how the local ordering may affect the oxygen ion diffusion mechanism in $NdBa_2Fe_3O_8$ compounds. We have seen that the oxygen diffusion coefficient is anticipated to be higher in the disordered cubic perovskite structure compared to the quintuple perovskite structure. We artificially created nanodomains of quintuple perovskite structures, being those domains coherently packed as observed by STEM [35]. In this case, we observe that the oxygen diffusion coefficient slightly increases compared to the extended quintuple perovskite structure, but the oxygen diffusion coefficient remains smaller compared to the disordered structure. The nanodomains considered here have a typical length of about 2 nm. In real materials, domains of several tens of nanometers have been reported, as observed through transmission electron microscopy (see Figure 2.b of ref. 35). We thus anticipate that real nanodomains of quintuple perovskite structure will essentially behave as a pure quintuple perovskite structure. As a whole, there is interest in having an extended cubic structure instead of locally chemically-twinned superstructure to favour oxygen diffusion. The obtention of disordered cubic phase supposes to make an effort during materials preparation to avoid, as far as possible, the ordering of cations on A-sites.

References

[1] Østergård, M.J.L., Clausen, C., Bagger, C., Mogensen, M., 1995. Manganite-zirconia composite cathodes for SOFC: Influence of structure and composition. Electrochimica Acta 40, 1971–1981. https://doi.org/10.1016/0013-4686(94)00332-U

[2] Østergård, M.J.L., Mogensen, M., 1993. ac Impedance study of the oxygen reduction mechanism on La1−xSrxMnO3 in solid oxide fuel cells. Electrochimica Acta 38, 2015–2020. https://doi.org/10.1016/0013-4686(93)80334-V

[3] Hansen, K.K., Wandel, M., Liu, Y.-L., Mogensen, M., 2010. Effect of impregnation of La0.85Sr0.15MnO3/yttria stabilized zirconia solid oxide fuel cell cathodes with La0.85Sr0.15MnO3 or Al2O3 nano-particles. Electrochimica Acta 55, 4606–4609. https://doi.org/10.1016/j.electacta.2010.03.017

[4] Hjalmarsson, P., Søgaard, M., Mogensen, M., 2008. Electrochemical performance and degradation of (La0.6Sr0.4)0.99CoO3−δ as porous SOFC-cathode. Solid State Ion. 179, 1422–1426. https://doi.org/10.1016/j.ssi.2007.11.010

[5] Bucher, E., Gspan, C., Sitte, W., 2015. Degradation and regeneration of the SOFC cathode material La0.6Sr0.4CoO3−δ in SO2-containing atmospheres. Solid State Ion. 272, 112–120. https://doi.org/10.1016/j.ssi.2015.01.009

[6] Choi, H.J., Bae, K., Jang, D.Y., Kim, J.W., Shim, J.H., 2015. Performance Degradation of Lanthanum Strontium Cobaltite after Surface Modification. J. Electrochem. Soc. 162, F622–F626. https://doi.org/10.1149/2.0971506jes

[7] Bucher, E., Gspan, C., Hofer, F., Sitte, W., 2013. Sulphur poisoning of the SOFC cathode material La0.6Sr0.4CoO3-δ. Solid State Ion. 238, 15–23. https://doi.org/10.1016/j.ssi.2013.03.007
[8] Sovacool, B.K., Turnheim, B., Hook, A., Brock, A., Martiskainen, M., 2021. Dispossessed by decarbonisation: Reducing vulnerability, injustice, and inequality in the lived experience of low-carbon pathways. World Dev. 137, 105116. https://doi.org/10.1016/j.worlddev.2020.105116
[9] Mancini, L., Eslava, N.A., Traverso, M., Mathieux, F., 2021. Assessing impacts of responsible sourcing initiatives for cobalt: Insights from a case study. Resour. Policy 71, 102015. https://doi.org/10.1016/j.resourpol.2021.102015
[10] Simner, S.P., Bonnett, J.F., Canfield, N.L., Meinhardt, K.D., Shelton, J.P., Sprenkle, V.L., Stevenson, J.W., 2003. Development of lanthanum ferrite SOFC cathodes. J. Power Sources 113, 1–10. https://doi.org/10.1016/S0378-7753(02)00455-X
[11] Hashim, S.S., Liang, F., Zhou, W., Sunarso, J., 2019. Cobalt-Free Perovskite Cathodes for Solid Oxide Fuel Cells. ChemElectroChem 6, 3549–3569. https://doi.org/10.1002/celc.201900391
[12] Zurlo, F., Di Bartolomeo, E., D'Epifanio, A., Felice, V., Natali Sora, I., Tortora, L., Licoccia, S., 2014. La0.8Sr0.2Fe0.8Cu0.2O3−d as "cobalt-free" cathode for La0.8Sr0.2Ga0.8Mg0.2O3−d electrolyte. J. Power Sources 271, 187–194. https://doi.org/10.1016/j.jpowsour.2014.07.183
[13] Baharuddin, N.A., Muchtar, A., Somalu, M.R., 2017. Short review on cobalt-free cathodes for solid oxide fuel cells. Int. J. Hydrog. Energy 42, 9149–9155. https://doi.org/10.1016/j.ijhydene.2016.04.097
[14] Kong, X., Zhou, X., Tian, Y., Wu, X., Zhang, J., Zuo, W., 2016. Niobium doped lanthanum calcium ferrite perovskite as a novel electrode material for symmetrical solid oxide fuel cells. J. Power Sources 326, 35–42. https://doi.org/10.1016/j.jpowsour.2016.06.111
[15] Chen, M., Paulson, S., Thangadurai, V., Birss, V., 2013. Sr-rich chromium ferrites as symmetrical solid oxide fuel cell electrodes. J. Power Sources 236, 68–79. https://doi.org/10.1016/j.jpowsour.2013.02.024
[16] Hong, G., Kim, T.W., Kwak, M.J., Song, J., Choi, Y., Woo, S.-K., Han, M.H., Cho, C.H., Kim, S.-D., 2020. Composite electrodes of Ti-doped SrFeO3-δ and LSGMZ electrolytes as both the anode and cathode in symmetric solid oxide fuel cells. J. Alloys Compd. 846, 156154. https://doi.org/10.1016/j.jallcom.2020.156154
[17] Tarancón, A., Burriel, M., Santiso, J., Skinner, S.J., Kilner, J.A., 2010. Advances in layered oxide cathodes for intermediate temperature solid oxide fuel cells. J. Mater. Chem. 20, 3799. https://doi.org/10.1039/b922430k
[18] Hu, Y., Hernandez, O., Broux, T., Bahout, M., Hermet, J., Ottochian, A., Ritter, C., Geneste, G., Dezanneau, G., 2012. Oxygen diffusion mechanism in the mixed ion-electron conductor NdBaCo2O5+x. J. Mater. Chem. 22, 18744. https://doi.org/10.1039/c2jm34396g
[19] Hermet, J., Dupé, B., Dezanneau, G., 2012. Simulations of REBaCo2O5.5 (RE=Gd, La, Y) cathode materials through energy minimisation and molecular dynamics. Solid State Ion. 216, 50–53. https://doi.org/10.1016/j.ssi.2011.11.006
[20] Tarancón, A., Morata, A., Dezanneau, G., Skinner, S.J., Kilner, J.A., Estradé, S., Hernández-Ramírez, F., Peiró, F., Morante, J.R., 2007. GdBaCo2O5+x layered perovskite as an intermediate temperature solid oxide fuel cell cathode. J. Power Sources, Hybrid Electric Vehicles 174, 255–263. https://doi.org/10.1016/j.jpowsour.2007.08.077
[21] Burriel, M., Peña-Martínez, J., Chater, R.J., Fearn, S., Berenov, A.V., Skinner, S.J., Kilner, J.A., 2012. Anisotropic Oxygen Ion Diffusion in Layered PrBaCo2O5+δ. Chem. Mater. 24, 613–621. https://doi.org/10.1021/cm203502s
[22] Zhou, Q., Wang, F., Shen, Y., He, T., 2010. Performances of LnBaCo2O5+x–Ce0.8Sm0.2O1.9 composite cathodes for intermediate-temperature solid oxide fuel cells. J. Power Sources 195, 2174–2181. https://doi.org/10.1016/j.jpowsour.2009.10.062
[23] Pelosato, R., Cordaro, G., Stucchi, D., Cristiani, C., Dotelli, G., 2015. Cobalt based layered perovskites as cathode material for intermediate temperature Solid Oxide Fuel Cells: A brief review. J. Power Sources, 298, 46-67. https://doi.org/10.1016/j.jpowsour.2015.08.034

[24] Beales, T.P., Mölgg, M., Jutson, J., Friend, C.M., 1997. Synthesis and Properties of YBaMn2O5+δ. Phys. Status Solidi A 161, 271–282. https://doi.org/10.1002/1521-396X(199705)161:1<271::AID-PSSA271>3.0.CO;2-2
[25] Jeamjumnunja, K., Gong, W., Makarenko, T., Jacobson, A.J., 2015. A determination of the oxygen non-stoichiometry of the oxygen storage material YBaMn2O5+x. J. Solid State Chem. 230, 397–403. https://doi.org/10.1016/j.jssc.2015.07.044
[26] Jeamjumnunja, K., Gong, W., Makarenko, T., Jacobson, A.J., 2016. A determination of the oxygen non-stoichiometry of the oxygen storage materials LnBaMn2O5+δ (Ln=Gd, Pr). J. Solid State Chem. 239, 36–45. https://doi.org/10.1016/j.jssc.2016.04.006
[27] Yamada, S., Sagayama, H., Yamazaki, M., Aoki, H., Sugimoto, K., Arima, T., 2022. Physical properties and phase diagram of single crystal REBaMn2O6 (RE = Sm, Eu, Gd, Tb, Dy, and Y). J. Solid State Chem. 315, 123504. https://doi.org/10.1016/j.jssc.2022.123504
[28] Karen, P., 2021. Oxygen nonstoichiometry in LnBaFe2O5+x across Ln = Nd, Sm, Gd. J. Solid State Chem. 301, 122297. https://doi.org/10.1016/j.jssc.2021.122297
[29] Karen, P., Woodward, P.M., 1999. Synthesis and structural investigations of the double perovskites REBaFe2O5+w (RE=Nd, Sm). J. Mater. Chem. 9, 789–797. https://doi.org/10.1039/a809302d
[30] Karen, P., 2006. Nonstoichiometry in oxides and its control. J. Solid State Chem. 179, 3167–3183. https://doi.org/10.1016/j.jssc.2006.06.012
[31] Huang, Q.Z., Lynn Karen, V., Santoro, A., Kjekshus, A., Lindén, J., Pietari, T., Karen, P., 2003. Substitution of Co3+ in YBa2Fe3O8. J. Solid State Chem. 172, 73–80. https://doi.org/10.1016/S0022-4596(02)00122-6
[32] Cordaro, G., Flura, A., Donazzi, A., Pelosato, R., Mauvy, F., Cristiani, C., Dotelli, G., Grenier, J.C., 2020. Electrochemical characterization of PrBa2−xSrxCu3O6+δ layered oxides as innovative and efficient oxygen electrode for IT-SOFCs. Solid State Ion., 348, 115286. https://doi.org/10.1016/j.ssi.2020.115286
[33] López-Paz, S.A., Marín-Gamero, R., Irujo-Labalde, X.M. de, Sánchez-Marcos, J., Perez-Coll, D., Franco, M.Á.A. y, García-Martín, S., 2021. YBaCuO-type perovskites as potential air electrodes for SOFCs. The case of YSr2Cu2FeO7+δ. J. Mater. Chem. A 9, 8554–8560. https://doi.org/10.1039/D1TA00111F
[34] Karen, P., Kjekshus, A., Huang, Q., Karen, V.L., Lynn, J.W., Rosov, N., Natali Sora, I., Santoro, A., 2003. Neutron powder diffraction study of nuclear and magnetic structures of oxidized and reduced YBa2Fe3O8+w. J. Solid State Chem. 174, 87–95. https://doi.org/10.1016/S0022-4596(03)00180-4
[35] Lindén, J., Karen, P., Kjekshus, A., Miettinen, J., Karppinen, M., 1999. Partial Oxygen Ordering in Cubic Perovskite REBa2Fe3O8+w (RE=Gd, Eu, Sm, Nd). J. Solid State Chem. 144, 398–404. https://doi.org/10.1006/jssc.1999.8178
[36] Volkova, N.E., Mychinko, M.Yu., Golovachev, I.B., Makarova, A.E., Bazueva, M.V., Zyaikin, E.I., Gavrilova, L.Ya., Cherepanov, V.A., 2019. Structure and properties of layered perovskites Ba1-xLnxFe1-yCoyO3-δ (Ln = Pr, Sm, Gd). J. Alloys Compd. 784, 1297–1302. https://doi.org/10.1016/j.jallcom.2018.12.391
[37] Zhou, Q., Chen, L., Cheng, Y., Xie, Y., 2016. Cobalt-free quintuple perovskite Sm1.875Ba3.125Fe5O15−δ as a novel cathode for intermediate temperature solid oxide fuel cells. Ceram. Int. 42, 10469–10471. https://doi.org/10.1016/j.ceramint.2016.03.174
[38] Martínez de Irujo-Labalde, X., Muñoz-Gil, D., Urones-Garrote, E., Ávila-Brande, D., García-Martín, S., 2016. Complex modulation of the crystal structure of a layered perovskite. A promising solid-oxide-fuel-cell cathode. J. Mater. Chem. A 4, 10241–10247. https://doi.org/10.1039/C6TA03307E
[39] Kundu, A.K., Yu Mychinko, M., Caignaert, V., Lebedev, O.I., Volkova, N.E., Deryabina, K.M., Cherepanov, V.A., Raveau, B., 2015. Coherent intergrowth of simple cubic and quintuple tetragonal perovskites in the system Nd2-xBa3+x(Fe,Co)5O15−δ. J. Solid State Chem. 231, 36–41. https://doi.org/10.1016/j.jssc.2015.07.050

[40] I.T. Todorov, W. Smith, K. Trachenko & M.T. Dove, 2006. DL_POLY_3: new dimensions in molecular dynamics simulations via massive parallelism. J. Mater. Chem. 16, 1911-1918. https://doi.org/10.1039/B517931A
[41] Cherry, M., Islam, M.S., Catlow, C.R.A., 1995. Oxygen Ion Migration in Perovskite-Type Oxides. J. Solid State Chem. 118, 125–132. https://doi.org/10.1006/jssc.1995.1320
[42] Calandrini, V., Pellegrini, E., Calligari, P., Hinsen, K., Kneller, G.R., 2011. nMoldyn - Interfacing spectroscopic experiments, molecular dynamics simulations and models for time correlation functions. Collection SFN 12, 201-232. https://doi.org/10.1051/sfn/201112010
[43] Hirel, P., 2015. Atomsk: A tool for manipulating and converting atomic data files. Comput. Phys. Comm. 197. 212-219. https://doi.org/10.1016/j.cpc.2015.07.012
[44] Parfitt, D., Chroneos, A., Tarancón, A., Kilner, J.A., 2011. Oxygen ion diffusion in cation ordered/disordered GdBaCo2O5+δ. J Mater Chem 21, 2183–2186. https://doi.org/10.1039/C0JM02924F
[45] Seymour, I.D., Tarancón, A., Chroneos, A., Parfitt, D., Kilner, J.A., Grimes, R.W., 2012. Anisotropic oxygen diffusion in PrBaCo2O5.5 double perovskites. Solid State Ion., 216, 41-43. https://doi.org/10.1016/j.ssi.2011.09.002
[46] Momma, K. and Izumi, F., 2011. VESTA 3 for three-dimensional visualization of crystal, volumetric and morphology data. J. Appl. Crystallogr. 44, 1272-1276. https://doi.org/10.1107/S0021889811038970